INTERNATIONAL JOURNAL FOR NUMERICAL METHODS IN FLUIDS, VOL. 24, 913–931 (1997)

A NUMERICAL MODEL FOR THREE-DIMENSIONAL RUN-UP

H. JOHNSGARD[1] AND G. PEDERSEN[1]*

[1]*Department of Mathematics, University of Oslo, Box 1053, N-0316 Oslo, Norway*

SUMMARY

A Lagrangian finite difference model for non-dispersive (long) and fully non-linear surface waves is presented. The Lagrangian description enables the inclusion of run-up and back-wash at sloping shores. The numerical procedure has been verified through a series of tests, including systematic grid refinements and comparison with analytical solutions for run-up.

Results for a few cases with moderately complex geometries are presented. The run-up distribution on an idealized headland is computed and discussed in view of the involved physical mechanisms. Some cases involve a time-dependent bottom topography, corresponding to a moving slide penetrating the fluid surface. The numerical solution procedure appears to be robust, unless wave breaking is encountered, and grid refinement tests show fast convergence once the scales in the problems are resolved.

The presented work has been carried out under the GITEC and GITEC-TWO projects that have been funded by the European Commission, under the contracts EVCV-CT92-0175, ENV4-U96-0297, and by the Norwegian Research Council. Int. j. numer. methods fluids 24: 913–931, 1997.

(No. of Figures: 12. No. of Tables: 0. No. of Refs: 21.)

KEY WORDS: run-up; Lagrangian co-ordinates; finite differences; slide-generated waves

1. INTRODUCTION

One of the major questions associated with surface waves on the sea is their eventual impact on the shore or marine constructions. The problem arises in a variety of contexts with important implications, ranging from disastrous tsunamis to bore sedimentation in the surf zone and erosion on the banks of canals due to waves generated by moving vessels.

In its full extent, including breaking, viscous effects, turbulence, influence of porous ground, interaction with vegetation and building, etc., the run-up topic inherits a complexity far beyond the limitations of the hydrodynamical theories and computational tools of today. Even when confined to non-breaking waves and laminar flow of inviscid fluid on a rigid impermeable bottom, no general theory or reliable numerical solution procedure has been established for the *complete* three-dimensional problem, including dispersion, non-linearity and sufficient resolution of complex bathymetry.

The simplest approach is to study two-dimensional run-up within the frame of hydrostatic shallow water theory. In the linear approximation a numerical solution is readily produced and for a few

* Correspondence to: G. Pedersen, Department of Mathematics, University of Oslo, Box 1053, N-0316 Oslo, Norway

Contract grant sponsor: European Commission; Contract grant numbers: EVCV-CT92-0175, ENV4-U96-0297
Contract grant sponsor: Norwegian Research Council

CCC 0271–2091/97/090913–19$17.50

Received December 1995
Revised August 1996

bottom profiles even analytical solutions are available. For a constant bottom slope, Carrier and Greenspan[1] applied combinations of Riemann invariants to transform the non-linear Airy equation into a linear wave equation. This technique, which today may be regarded as nearly classical, is still widely in use, often in combination with patching to linear offshore solutions.[2–5] One surprising result is that the linking of the Carrier and Greenspan technique to linear incident waves yields extremes for the shoreline motion that are exactly reproduced when linear theory is used throughout.[3,6] Naturally, when a wave is close to breaking, the long-wave assumption behind the Carrier and Greenspan technique becomes invalid in strict terms and a restriction is put on the amplitude of the incident wave. For an incident pulse of finite length, breaking occurs most easily during the withdrawal of the shoreline. However, as shown by comparison with experiments, another peculiar feature of the theory is its apparent ability to predict the breaking criterion with rather good accuracy.[3,4]

A few other exact solutions are also known. Of particular relevance to the present work are the exact non-linear solutions, including run-up, for eigen-oscillations in parabolic basins reported by Thacker.[7]

The crucial point in numerical simulations of wave run-up is the tracking of the moving shoreline and adaptation of the computational domain to properly reproduce the actual fluid domain. A common approach is based on the non-linear hydrostatic equations discretized on a fixed Eulerian grid covering the fluid as well as the land adjacent to the shore. The equations are solved in the wet region that is dynamically modified according to the motion of the shoreline. This yields a scheme that can handle complex geometries very efficiently with a strong non-linear representation of the shoreline. It has been applied with good results in e.g. References 8–10. However, methods of this kind rely crucially on extrapolation at the shore, which in turn requires the implementation of a rather strong damping, either as an explicit friction term or inherent in the basic numerical technique itself, as with the Lax–Wendroff scheme. The effect of this damping in combination with the first-order errors due to the interpolation is difficult to control, especially in three-dimensional calculations where saw-tooth boundaries are likely to create problems. As demonstrated in Reference 11, such boundaries often create severe noise and artificial diffraction in coastal regions, even for purely linear calculations.

Our strategy is to apply a Lagrangian description based on the assumption that the moving shoreline is material in the sense that it always contains the same fluid particles. For an ideal fluid this requirement is met provided that the angle of the fluid wedge at the 'shore tip' is well below 90°, as will be the case for run-up of waves that are far from breaking. In References 12–14, long-wave run-up has been computed by means of Lagrangian co-ordinates. Most of the attention was devoted to non-linear dispersive waves in narrow channels, which yield essentially two-dimensional motion that was described by Boussinesq-type equations. However, Reference 12 also contained a preliminary discussion of three-dimensional run-up that is closely related to the content of the present paper. Herein we use the notation 'three-dimensional' for problems that physically involve fluid motion in three dimensions. Certainly, there is then wave propagation in two dimensions and any long-wave theory becomes only two-dimensional mathematically. In References 12–14, care was taken to ensure a strong non-linear description of the shoreline. Later, Zelt and Raichlen[15] presented a finite element technique for the solution, in complex geometries, of a set of three-dimensional Boussinesq equations in Lagrangian co-ordinates. As opposed to References 12–14 the method of Zelt and Raichlen involved features such as series expansion at the beach that render the technique only weakly non-linear.

A full, inviscid description of two-dimensional wave run-up is provided by boundary element/panel methods.[16,17] Generally the description again is Lagrangian, or semi-Lagrangian at

least, in the sense that fluid particles at the free surface are traced. So far, no effective three-dimensional method of this kind has been reported.

2. BASIC EQUATIONS

Marking dimensional quantities by a superscript asterisk, we introduce a co-ordinate system with horizontal axes Ox^* and Oy^* at the undisturbed water level and Oz^* pointing vertically upwards. Further, we assume a bottom at $z^* = -h^*$ and denote the surface elevation and averaged horizontal particle velocity by η^* and $\mathbf{v}^*$ respectively. Applying the maximum depth h_0^* and a typical wavelength L^* as 'vertical' and 'horizontal' length scales respectively, we are then led to the definition of non-dimensional variables

$$\begin{aligned} x^* &= L^* x, \qquad y^* = L^* y, \qquad t^* = L^*(g h_0^*)^{-1/2} t, \\ \eta^* &= h_0^* \eta, \qquad z^* = h_0^* z, \qquad \mathbf{v}^* = (g h_0^*)^{1/2} \mathbf{v}, \end{aligned} \tag{1}$$

where g is the constant of gravity. Provided that $\beta \equiv (h_o^*/L^*)^2$ is sufficiently small, the wave motion can be governed by the long-wave equations. To trace the moving coastline automatically, we formulate the equations in a Lagrangian description. The Lagrangian enumeration co-ordinates a and b are introduced through the transformation

$$a_t + \mathbf{v} \cdot \nabla a = 0, \quad a(x, y, 0) = a_0(x, y), \qquad b_t + \mathbf{v} \cdot \nabla b = 0, \quad b(x, y, 0) = b_0(x, y), \tag{2}$$

where $\mathbf{v}$ is the averaged (in depth) horizontal velocity, ∇ is the horizontal component of the gradient operator and the index t denotes temporal differentiation. Often the initial conditions a_0 and b_0 are replaced by x and y respectively. Other choices for a_0 and b_0 really correspond to curvilinear Lagrangian co-ordinates. We note that the use of curvilinear Lagrangian co-ordinates does not lead to additional terms in the equations, since Lagrangian co-ordinates in any case can be regarded as set of time-dependent curvilinear co-ordinates relative to a fixed Eulerian frame of reference. The continuity equation now becomes

$$H \frac{\partial(x, y)}{\partial(a, b)} = V, \tag{3}$$

where $H \equiv h + \eta$ is the total water depth and

$$V = H(a, b, 0) \left. \frac{\partial(x, y)}{\partial(a, b)} \right|_{t=0}. \tag{4}$$

The quantity V has the interpretation of volume density per area in the (a, b) plane and we note that equation (3) explicitly expresses volume conservation for a vertical material fluid column. Using (3), we obtain momentum equations of the form

$$\frac{\partial^2 x}{\partial t^2} = -\frac{H}{V} \frac{\partial(\eta, y)}{\partial(a, b)}, \qquad \frac{\partial^2 y}{\partial t^2} = -\frac{H}{V} \frac{\partial(x, \eta)}{\partial(a, b)}. \tag{5}$$

By further application of (3) we may recast the momentum equations into conservative form. We display only the x-component, which reads

$$V \frac{\partial^2 x}{\partial t^2} = -\frac{\partial}{\partial a}\left(\frac{1}{2} H^2 \frac{\partial y}{\partial b}\right) + \frac{\partial}{\partial b}\left(\frac{1}{2} H^2 \frac{\partial y}{\partial a}\right) + V \frac{\partial h}{\partial x}. \tag{6}$$

As for other long-wave equations, the vertical motion is represented through the surface elevation η. Since the horizontal velocity is vertically uniform in the hydrostatic approximation, it readily follows that the vertical displacement will be linear in the vertical Lagrangian co-ordinate c:

$$z = \eta + \frac{H(a, b, t)}{H(a, b, 0)}(c - \eta(a, b, 0)). \tag{7}$$

In long-wave models the dominant frictional effects may be introduced by means of a horizontal bottom drag, which is generally modelled as a drag coefficient times a quadrature of the velocity. In the present model this standard representation must be modified at the shore to avoid infinite acceleration due to $H \to 0$. The bottom friction is essential when modelling the flooding of large plains with very gentle slopes, such as river deltas, valleys, etc. However, the success of a model then depends crucially on the correct tuning of the drag coefficient to reproduce the effect of bottom 'roughness' (vegetation, etc.) and other sources of energy loss. For steeper slopes, with inclination of at least a few degrees, say, and large-scale waves the effect of bottom drag may be small. On the other hand, small-scale run-up, as in most laboratory experiments, may be markedly influenced by frictional (viscous) effects even for steep slopes. This topic is discussed in Reference 13. In the present paper we focus on the representation on the moving shoreline and thus leave the inclusion of a bottom drag to future works. Moreover, run-up of large waves on gently sloping beaches must also be expected to produce turbulence of noticeable intensity throughout the fluid layer. Hence we must anticipate that there will be some diffusion of horizontal momentum due to eddy viscosity. Even though the effect on the overall characteristics of the solution is probably small, the eddy viscosity may affect small-scale features due to topography or diffraction. Often the inclusion of a diffusion term is desirable from a numerical point of view even when the physical significance is debatable. To some extent this is the case in the present work, where we experience a spurious production of edge waves for coarse grids. However, in the present context we prefer to remove the problem by a purely numerical remedy, namely a grid-dependent filtering akin to the effect of diffusion. The filter is described at the end of Section 3. Naturally, if the noise had been of a physical origin, it would have best been treated by an eddy viscosity term. Finally we note that the inclusion of a quadratic bottom drag by no means yields a selective damping of short waves and will thus be useless as a measure against noise.

3. NUMERICAL METHOD

We denote a discrete approximation to a function f at $a = i\Delta a$, $b = j\Delta b$ and $t = p\Delta t$ by $f = f_{i,j}^{(p)}$. The computational domain is divided into material fluid cells with a η-node in the middle and x- and y-nodes at the corners, as shown in Figure 1. This arrangement, which is well suited for calculations of Jacobian determinants, is often referred to as an Arakawa B grid.[18] The primary unknowns are

$$\eta_{i,j}^{(p)}, \quad H_{i,j}^{(p)}, \quad x_{i+1/2,j+1/2}^{(p)}, \quad y_{i+1/2,j+1/2}^{(p)}. \tag{8}$$

To abbreviate the expressions and improve their legibility, we define a symmetric difference operator δ_a and a midpoint average operator $\bar{f}^a$ according to

$$\delta_a f_{i+1/2,j}^{(p)} = \frac{f_{i+1,j}^{(p)} - f_{i,j}^{(p)}}{\Delta a}, \qquad \overline{f_{i+1/2,j}^{(p)}}^{a} = \frac{f_{i+1,j}^{(p)} + f_{i,j}^{(p)}}{2}. \tag{9}$$

The difference and average operators with respect to the other co-ordinates are defined correspondingly. We also collect terms within square brackets leaving the common indices outside.

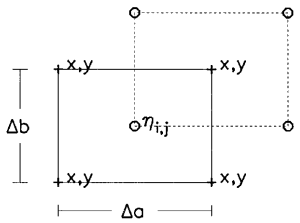

Figure 1. Spatial distribution of grid cells. Circules indicate nodes for surface elevation, while nodes for horizontal displacement are depicted with crosses. Full and broken rectangles mark the borders of control volumes for mass and momentum conservation respectively

The numerical method is explicit in time and the computational cycle starts with the calculation of a new generation of H-values from the updated displacement field x and y through a discrete version of (3) that reads

$$[H = V/J]_{i,j}^{(p)}, \quad \text{where } [J = \delta_a \bar{x}^b \delta_b \bar{y}^a - \delta_a \bar{y}^b \delta_b \bar{x}^a]_{i,j}^{(p)}. \tag{10}$$

The quantity $V_{i,j}$, which represents the volume of the computational cell, is simply the product of H and J at $t = 0$. New values for the surface elevation η may now be obtained from

$$[\eta = H - h(\bar{x}^{ab}, \bar{y}^{ab})]_{i,j}^{(p)}. \tag{11}$$

As the last step in each time cycle we discretize the momentum equations. The simplest option is to represent (5) directly according to

$$\left[\delta_t^2 x = -\frac{\bar{H}^{ab}}{\bar{V}_0^{ab}}(\overline{\delta_a \eta \delta_b y}^b - \overline{\delta_b \eta \delta_a y}^a)\right]_{i+\frac{1}{2},j+\frac{1}{2}}^{(p)}, \tag{12}$$

supplemented by a corresponding discrete y-component. Alternatively we have also employed discrete versions of the conservative formulation (6),

$$[V\delta_t^2 x = -\delta_a(\tfrac{1}{2}\overline{(H^2)}^b \delta_b \bar{y}^{ab}) + \delta_b(\tfrac{1}{2}\overline{(H^2)}^a \delta_a \bar{y}^{ab}) + V\{h_x\}]_{i+1/2,j+1/2}^{(p)}, \tag{13}$$

where different representations of the bottom pressure term h_x have been attempted. The two first terms on the right-hand side represent the vertically integrated pressure on the boundaries of the momentum conservation cell in Figure 1.

We adapt a curvilinear grid (see discussion below (2)) to make a possibly curved shoreline pass through a line of H-nodes at $i = 0$, say. The choice (12) for the momentum equation then involves η-values at the shoreline. These values are found by invoking $H = 0$ and linearly extrapolated values for x and y in (11) for $i = 0$. In the conservative formulation we employ the boundary condition $H_{0,j}^{(n)} = 0$ directly, whereas the term h_x is calculated either by differentiating the depth function or by finite differences, again involving some sort of extrapolation at the shoreline. We have performed a large number of tests of the two formulations with a variety of more or less sophisticated implementations of the bottom pressure term h_x. So far we have found no indications that the simpler non-conservative option is markedly inferior in any respect. Hence we employ (12) in the subsequent sections.

Along boundaries with a non-vanishing fluid depth a no-flux condition applies. In this paper only straight boundaries are considered and the no-flux condition is easily implemented through relations of symmetry.

For a constant depth h and uniform grid ($a_0 = \gamma_x x$, $b_0 = \gamma_y y$ in (2)) the linearized version of the difference equations (10)–(12) yields the CFL stability criterion $\sqrt{h}\Delta t < \min(\Delta x, \Delta y)$, where

$\Delta x = \Delta a/\gamma_x$, etc. To second order in the grid increments the numerical dispersion relation may be written as

$$\omega^2 = h\left[k^2 + l^2 + \frac{h\Delta t^2(k^2+l^2)^2}{12} - \Delta x^2\left(\frac{k^4}{12} + \frac{k^2 l^2}{4}\right) - \Delta y^2\left(\frac{l^4}{12} + \frac{k^2 l^2}{4}\right) + \text{h.o.}\right], \tag{14}$$

where the phase function is defined according to $\chi = kx + ly - \omega t$.

When a wave propagates in shoaling water, the wavelength decreases and the relative importance of the error terms in (14) increases. Under some extra assumptions we may quantify this effect. If the x-axis, say, corresponds to the principal offshore direction and the waves are fairly close to normal incidence, the theory of geometrical optics applied to the exact analytical dispersion relation yields $k \sim h^{-1/2}$, while l and the frequency remain constant. Thus in shoaling water the dominant contribution to the relative error in ω^2, as given by (14), becomes $\Delta x^2 k^4/12(k^2 + l^2) \sim \Delta x^2/h$. Hence a non-uniform grid yields an improved overall accuracy provided that the local Δx is proportional to $h^{1/2}$, which corresponds to $\partial a_0/\partial x \sim h^{-1/2}$, while a selective refinement in the direction y, or rather b, is less crucial. However, we note that the arguments are based on a simple geometry and the applicability of geometrical optics, which becomes invalid at the shoreline. In all the three-dimensional simulations reported herein we employ grids that yield local Δx close to $h^{1/2}$, except for the grid points adjacent to the shore where a specified minimum grid increment is invoked. When comparing with more uniform resolutions, we indeed observe that the refined grids yield a substantial improvement in the overall solution. However, the grid size must have a certain minimum value to avoid critical effects of round-off errors at the shore.

For most non-linear numerical methods we will observe that the solution eventually becomes severely contaminated by noise for large simulation times, a phenomenon that is often referred to as aliasing. For the present method we will subsequently encounter another mechanism for noise production, namely artificial diffraction to short waves at the shoreline. In three-dimensional simulations this effect will generally appear long before ordinary aliasing. Naturally, in the end the effects may combine to accelerate a global breakdown. In order to avoid the production of noise of either origin, one may apply some kind of filtering. Herein we have tested a simple three-point smoothing where the relation between the filtered value $\hat{f}$ and the original discrete field f can be written in either of two ways,

$$\hat{f} = \bar{f}^{xx} \quad \text{or} \quad \hat{f} - f = \frac{\Delta x^2}{4}\delta_x^2 f. \tag{15}$$

The latter expression demonstrates the interpolation of the filtering as the action of an artificial diffusion in the governing equations, implemented through a kind of split step scheme. When filtering a two-dimensional field, the procedure is applied along both grid directions. As a result, the noise on the grid scale is completely annihilated, while long-wave components experience a slight damping only. The filtering is involved only at some of the time steps and is never applied to quantities such as H that contain the equilibrium depth. At a boundary we employ the asymmetric three-point formula $\hat{f}_j = \frac{1}{4}(3f_j + 2f_{j+1} - f_{j+2})$. The spatial Nyquist wave is still annihilated.

4. VERIFICATION AND TESTS

4.1. Tests

Several tests have been applied to the computer code based on the present model.

1. The conservation of mass and energy. Mass is conserved exactly by the numerical scheme; mass conservation in the simulation then confirms the validity of the code. As expected, energy

is conserved to second order in the computations, with no systematic gain or loss, unless the smoothing procedure is applied.

2. Comparison with non-linear eigensolutions for a parabolic basin, as reported in Reference 7. The first mode is easily generalized to the 3D case with an arbitrarily shaped shoreline. This solution is reproduced exactly, within round-off errors, by the numerical method. Oscillations about both the x- and y-axis have been implemented to verify the computer code further.
3. Comparison with non-linear solutions for run-up on a straight slope, as reported in Reference 1. The numerical method reproduces these results with good accuracy even for cases close to breaking. Further details are given in Section 4.2.
4. The numerical representation of steepening. When propagating in water of constant depth, wave pulses eventually develop hydraulic jumps. The exact solution of the Airy equations, easily found by the method of characteristics, breaks and becomes multivalued. The numerical scheme reproduces this solution with second-order accuracy, until the wave front consists of a few grid points only. Adjacent to the front, noise on the grid scale then appears. Naturally, the breaking itself is not reproduced.
5. Grid refinement tests. Such tests have been carried out for all the simulations reported herein. The convergence was of second order except for the noise on the grid scale following the main wave pulses (see discussion below).

Owing to numerical dispersion, propagating wave pulses emerging from the initial conditions are followed by a tail of waves with lengths of the order of the grid increment. Their amplitudes depend on the tails of the spectra and turn out to be somewhere between first and second orders in the grid increments for the reported simulations. Hence the second-order accuracy does not hold here. We notice that any finite difference or element method inherits the same feature.

4.2. Comparison with an analytical solution

In 1958 Carrier and Greenspan[1] published an analytical treatment of the hydrostatic and fully non-linear run-up on an inclined plane. The assumption of constant bottom slope enabled an ingenious transformation, using Riemann invariants, to a linear problem. Recently the theory has been generalized to include run-up in channels with parabolic cross-sections.[19] We will not go much into the particulars of the theory, but focus on one fundamental solution only.

Assuming $h^* = vx^*$ and a characteristic time scale T, we select typical length scales according to

$$L = gT^2v, \qquad h_0 = gT^2v^2, \tag{16}$$

which gives $h = x$. Carrier and Greenspan arrived at the linear wave equation

$$\frac{\partial}{\partial\sigma}\left(\sigma\frac{\partial\phi}{\partial\sigma}\right) - \sigma\frac{\partial^2\phi}{\partial\lambda^2} = 0, \tag{17}$$

where the transformation to physical quantities can be expressed as

$$\begin{aligned} u &= -\sigma^{-1}\partial\phi/\partial\sigma, & \eta &= \tfrac{1}{4}\partial\phi/\partial\lambda - \tfrac{1}{2}u^2, \\ t &= \tfrac{1}{2}\lambda + u, & x &= -\tfrac{1}{4}\partial\phi/\partial\lambda + \tfrac{1}{16}\sigma^2 + \tfrac{1}{2}u^2. \end{aligned} \tag{18}$$

Choosing T so as to give a non-dimensional frequency equal to 2, we may write a standing wave solution of (17) according to

$$\phi = A\mathrm{J}_0(\sigma)\cos\lambda, \tag{19}$$

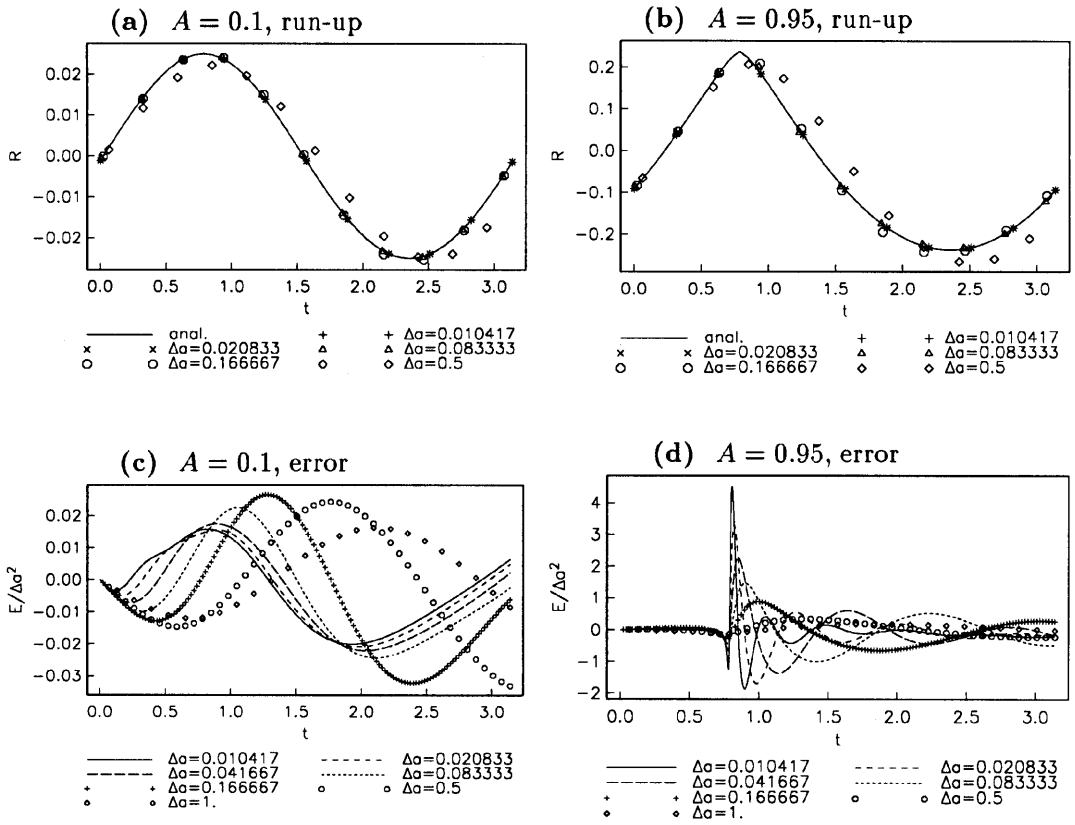

Figure 2. Comparison with analytical standing wave solution

where J_0 is the Bessel function of zeroth order and A is an amplitude factor. For $A > 1$ the transformations in (18) become multivalued as an indication of wave breaking. We obtain the solution in the physical plane by converting the algebraic equations in (18) by means of an iterative solver. Combining this solver with a Runge–Kutta technique, we may also obtain particle trajectories corresponding to the Lagrangian description. Within a domain of roughly $x < 10$ we have performed simulations in double precision with different values of A. As expected, the convergence is generally much faster in deep water than at the shoreline. Run-up values for $A = 0{\cdot}1$ and $0{\cdot}95$ are displayed in Figures 2(a) and 2(b) respectively. We observe good convergence even for the amplitude $A = 0{\cdot}95$, which is fairly close to the breaking limit ($A = 1$). To control the convergence order, we have also depicted the error E in the run-up divided by Δa^2; see Figures 2(c) and 2(d). For the nearly linear case $A = 0{\cdot}1$ we clearly observe the expected quadratic convergence. However, for $A = 0{\cdot}95$ the convergence is not quite quadratic, though it is much faster than linear. In fact, a good fit to the leading error is const. $\times \Delta a^2 \ln(\Delta a)$, at least for the maximum value. Naturally, for practical purposes such a convergence rate may be regarded as quadratic.

5. EXAMPLE 1. INCIDENT WAVES IMPINGING ON A HEADLAND

5.1. Geometry and set-up

We have chosen a simple set-up for this example. The incident wave is a plane wave with a trigonometric hat shape that is specified in a region of constant depth. As an idealized model of the coastline we employ a symmetric bell-shaped point adjoined at each side by a straight coastline. The bottom is sloping monotonically from the coast until the constant depth of the offshore region is attained. Since the geometry as well as the incident wave is symmetric, we perform calculations in half the domain only. In the present context it is convenient to employ a horizontal length scale L linked to the slope, while the constant depth h_0 of the offshore region is used to make the surface elevation dimensionless. Accordingly, the time scale becomes $L/\sqrt{(gh_0)}$. When presenting numerical results, L will be chosen so as to give bottom slopes of unit inclination. However, to make the contents of equations and formulae more transparent, we will retain a general bottom slope in the introductory discussions. We may then express the incident wave through requiring zero velocity and imposing an initial surface elevation of the form

$$\eta_{\text{in}} = A[1 + \cos(k(x - x_i))] \quad \text{for } |k(x - x_i)| < \pi. \tag{20}$$

This initial condition leads to an incident pulse of total length $\lambda \equiv 2\pi/k$ and, in the linear approximation, amplitude A.

The bottom topography is depicted in Figure 3. A bottom profile at constant y contains a section of constant slope adjoined continuously with a flat bottom. The computational domain is confined to $0 < y < y_{\text{p}}$. At $y = y_{\text{p}}$ we introduce one half of a Gaussian-shaped peninsula implicitly completed by the application of a symmetry condition. The bottom function is defined according to

$$h(x, y) = q(x - s(y)), \quad s(y) = B \exp\left[-\left(\frac{y - y_p}{r}\right)^2\right], \tag{21}$$

where the depth profile q is constructed by adjoining a flat bottom and a linear slope by a quadratic polynomial to obtain a continuously differentiable function. Denoting the halfwidth of the transition interval by l, we may then write

$$q(\xi) = \begin{cases} \tan\theta\xi & \text{if } \xi < \cot\theta - l, \\ 1 - (\tan\theta/4l)(\xi - \cot\theta - l)^2 & \text{if } -l < \xi - \cot\theta < l, \\ 1 & \text{if } \xi > \cot\theta + l. \end{cases} \tag{22}$$

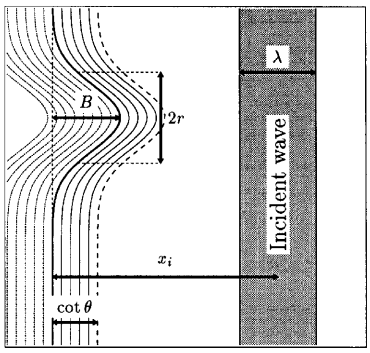

Figure 3. Definition sketch of idealized headland geometry. The increment of the depth contours 0·2 and the equilibriunm shoreline is depicted with the bold full line

In all the reported simulations the transition interval is very small, corresponding to $l = 0{\cdot}01 \cot\theta$. Tests reveal no noticeable dependence on l for such small values. In fact, most hydrostatic simulations may probably be run with $l = 0$ with no other consequences than a faint and local fluctuation of the surface above the transition point. This may be different if dispersive effects are taken into account, as in Boussinesq- or KdV-type equations.

5.2. *Governing parameters for run-up*

In the previous subsection we defined an apparently simple run-up problem. Still, a discussion of the quantitative variations with the parameters and the involved physical mechanisms becomes rather rich. Thus, in addition to being instructive in itself, it may serve as a warning against uncritical quantitative transference of results for idealized cases to a really complex context. For the geometry and incident wave described above, the run-up height depends on the parameters A, λ, B, r, θ, l and x_i. Since the long-wave equations are invariant with respect to the choice of L, we immediately realize that the run-up height may depend on λ and θ only in the combination $\lambda_e = \lambda \tan\theta$ in the hydrostatic approximation. As long as l is rather small, we may assume that the actual value has very little influence on the run-up height. We may then assume a relation of the form

$$\frac{R}{A} = f(\lambda_e, \beta, A, B, r, y, x_i), \tag{23}$$

where R is the run-up height. The most critical parameter is λ_e. At a straight coast (no dependence on B, r, y), f is close to 2 in the limit $\lambda_e \to \infty$ corresponding to a vertical wall. If λ_e is reduced, f increases, as long as breaking is not encountered, implying that of two incident waves of equal amplitude the shortest one will give the largest run-up. This may be at least partly understood from the general behaviour of waves in a varying medium. A short incident wave will experience the deeper part of the slope as slowly varying, with a correspondingly negligible reflection of energy. At the shore, on the other hand, we have a singularity in the equations and the medium may never be regarded as slowly varying. Then it is reasonable to assume that a shorter wave will have its reflection more confined to the close vicinity of the moving shoreline, thereby giving a larger run-up.

The value of f is much less sensitive to A as long as we are well clear of the breaking regime. In fact, A has influence primarily in combination with the distance x_i that enters the relation owing to evolution of the incident wave over the portion of flat bottom before the slope starts. Analytical techniques that patch a fully non-linear, hydrostatic solution over the slope to a linear solution in the offshore region yield an f that is perfectly independent of A.[3] A closer study will lead us to assume that A influences f through steepening of the incident wave, which causes a shorter front and a smaller effective λ_e. The role of a small β, which measures the importance of dispersion (defined below equation (1)), is similar in some respects. Dispersion effects are not likely to be important close to the shore owing to the vanishing water depth. However, if dispersion is important during propagation over deep water, it will reduce the run-up height when combined with a sufficiently large x_i.

We now turn to the consideration of the parameters connected to the three-dimensionality, namely B, r and y. First we note that the non-linearity and dispersion will have a shorter time to influence the wave before it reaches the slope outside the point than outside the straight coastline. The difference will correspond to a reduction of x_i. Naturally, the curved coastline will also alter the effective bottom slope angle. We will confine the further discussion to a few asymptotic cases. For a gently varying geometry, λ_e, $\lambda/r \ll 1$, we may apply the well-known results from geometric and physical optics that

* For solitons the Mach stem may reach a height four times that of the incident wave.[20] A possible effect of this kind is reported by Wiegel[21] for a tsunami at Hilo, Hawaii, 1946.

predict focusing at the point, with a corresponding increase in f, and defocusing at the adjacent 'bay'. Even though this result is generally derived for linear waves, it will obviously hold for larger A as well. Another limiting case is defined by λ_e and B/r being large, corresponding to steep slopes and a narrow, wedge-like point. In this case f will be close to unity at the point and a reflection pattern starts to evolve as the wave propagates along the bill. If B is large compared with λ, this will produce a marked maximum for f at the base of the peninsula. For large A at this effect may be increased further by the Mach stem effect.* Thus for intermediate parameter values the qualitative characteristics of the amplitude distribution at the peninsula are not easily determined without doing the actual calculations. For the back-wash, secondary run-up, etc. the matter will be further complicated by the diffraction from the point and generation of edge waves.

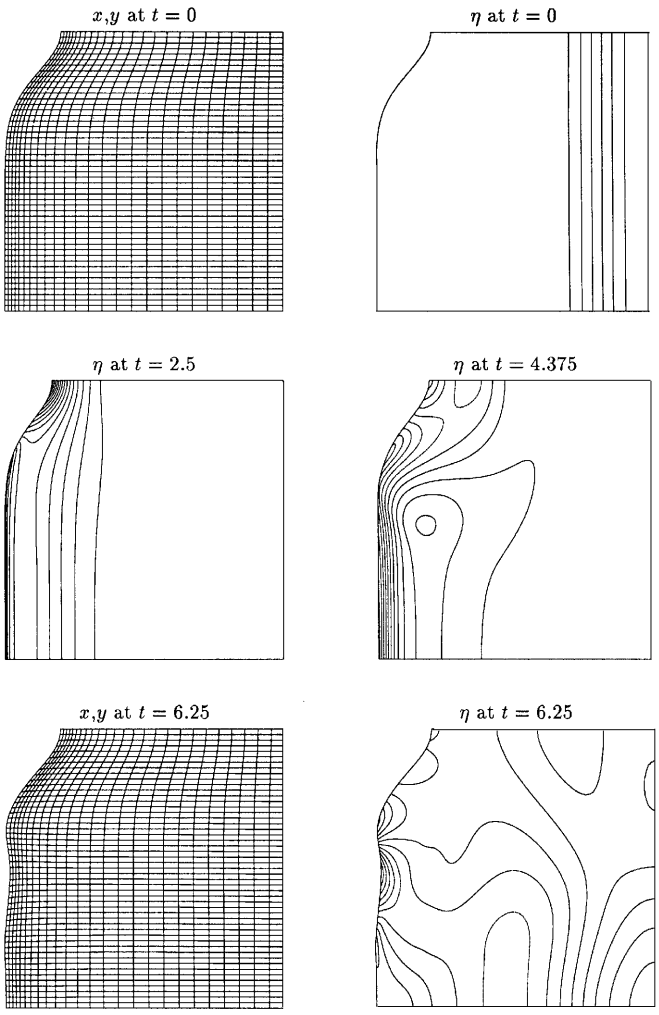

Figure 4. Contour plots of surface (increment 0·005) and wire plots for displacement field, displaying one of four points in each direction

5.3. Simulations

In addition to the shoreline, the computational domain is confined by lines of symmetry, corresponding to no-flux conditions, at the three lines $b = y = y_p$ (at the point of the peninsula), $b = 0$ and $a = x_i$. The second boundary will give artificial reflections of diffracted waves from the point, while the last will reflect the main outgoing pulse from the shore. The simulations are stopped before these reflections become important. Naturally, this could have been avoided by the introduction of radiation conditions of absorbing ('sponge') domains in the vicinity of the boundary. However, the performance of the run-up model is demonstrated equally well without such conditions.

We will display results for two selected cases and select L so as to give a slope length $\cot\theta = 1$. Accordingly, λ now becomes identical with λ_e defined in the preceding subsection. Moreover, we choose $x_i = 1 + B + \frac{1}{2}\lambda$ for both cases. The results in Figure 4 then correspond to the parameters $\lambda = 2, A = 0{\cdot}0175, B = r = 0{\cdot}5$ and $y_p = 2{\cdot}5$. These parameters are rather typical for slide-generated waves in a fjord or lake, but the incident waves are too high and long (in relation to the bottom slope) as compared with most tsunamis originating in deep sea. In the figure we have displayed the displacement field and surface elevations at selected times. We notice in particular the large amplitudes and deformations due to the generated edge waves at $t = 6{\cdot}25$.

At the shore we have extracted the run-up height R as function of the lengthwise Eulerian co-ordinate y. As shown in Figure 5(a), the present case yields an appreciable amplification at the point due to focusing. Adjacent to the point we observe an equally pronounced reduction of R.

In Figure 5(b) we have displayed the distribution of maximum run-up for a simulation with the parameters $\lambda = 8, A = 0{\cdot}02, B = 2, r = 1$ and $y_p = 9$. The most important difference from the previous case is the narrower shape of the peninsula and the larger wavelength/slope length ratio, leading to less pronounced amplification and focusing effects (see Section 5.2). In fact, we now observe a run-up height with a minimum ($R/A = 1{\cdot}44$) near the point ($y = 8{\cdot}78$), a maximum ($R/A = 3{\cdot}01$) at the outskirts of the headland and a constant value ($R/A = 2{\cdot}43$) further away at the plane shore.

For the simulations reported herein, the CPU time consumed, T_{cpu}, becomes roughly proportional to the number of grid points times the number of time steps. Denoting the grid dimensions by N, M and P in a, b and t respectively, we may then write $T_{cpu} = \kappa_c NMP$. On the mid-range workstation SGI-Indy with R4610 FPU and 100 MHz R4600 CPU we obtain $\kappa_c \approx 3{\cdot}6 \times 10^{-5}$ s. For a typical simulation with a fine grid, corresponding to $N = 100, M = 200$ and $P = 1000$, say, we then obtain $T_{cpu} = 12$ min. The subsequent examples yield an approximate CPU time reduction of 15% owing to

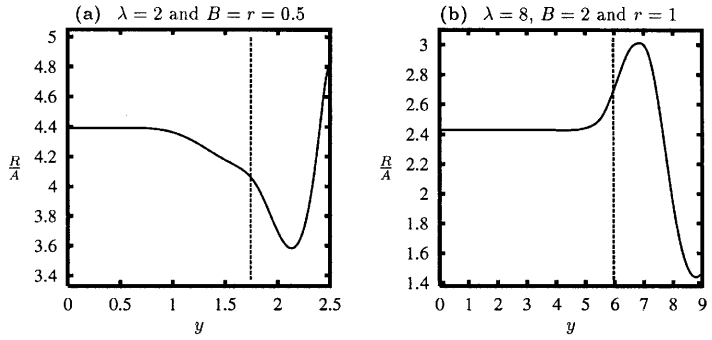

Figure 5. Maximum amplification factor R/A along coastline. Vertical broken lines indicate the positions at which the equilibrium shore is displaced by $0{\cdot}1B$ as compared with the straight coast. (a) Case displayed in Figure 4. (b) Case with 'steep' slope

a simpler depth function. On the more powerful workstation IBM RS6000/990 we observe that the CPU time is typically reduced by a factor of four.

5.4. *Grid refinement tests*

We will briefly present grid refinement tests for both geometries employed above. Since we have a non-uniform grid, we identify the resolutions by average grid increments that are defined according to $\Delta x = x_i/N$ and $\Delta y = y_p/M$, where N and M are the numbers of points in the a- and b-direction respectively. For all solutions reported, we have $\Delta x = \Delta y/2$, although computations have also been performed for other ratios. Results are presented for increments in the range $0{\cdot}0125 < \Delta x < 0{\cdot}28$. Guided by Section 4.2, we focus on the discrete representation of the shoreline.

For the case displayed in Figure 4, we found that the solutions converged rapidly and that they remained smooth even for rather coarse grids (Figure 6). However, the narrower peninsula ($B = 2, r = 1$), for which results are displayed in Figure 5(b), corresponds to more severely strained grids. As shown in Figure 8(a), coarse resolutions now yield a significant generation of grid-scale noise along the peninsula. According to Figure 7(a), the phenomenon is primarily confined to the vicinity of the shore. Moreover, further investigations indicate that the short-scale disturbances are progressive with a small celerity and that they grow only during the impact of the incident wave. Naturally, a series of impacts, as for a periodic incident wave, may then give an accumulation of small-scale disturbances. A case with reduced amplitude $A = 0{\cdot}0002$ is depicted in Figure 8(b). Surprisingly, whereas the overall convergence is improved, owing to decreased wave steepness close to the shore, the generation of noise is not substantially reduced. This implies that the spurious phenomenon stems from linear effects. Hence the noise is probably best interpreted as a diffraction to short edge waves due to the grid-scale inhomogeneity of the discrete representation of the near-shore region. We note that the grid must be refined in both directions to suppress the noise production, whereas the convergence of the large-scale features depends most crucially on the resolution in the offshore direction.

As an alternative to employing very fine grids, the contamination of the solution by short waves in the shore zone may be inhibited by the filtering described by (15). In Figure 8(d) we have compared some of the unfiltered solutions with solutions where the numerical filter has been applied to the velocity field at each 25th time step only. Even for the coarser grid the noise is annihilated, while the overall influence on the solution anyway is less than the discretization error.

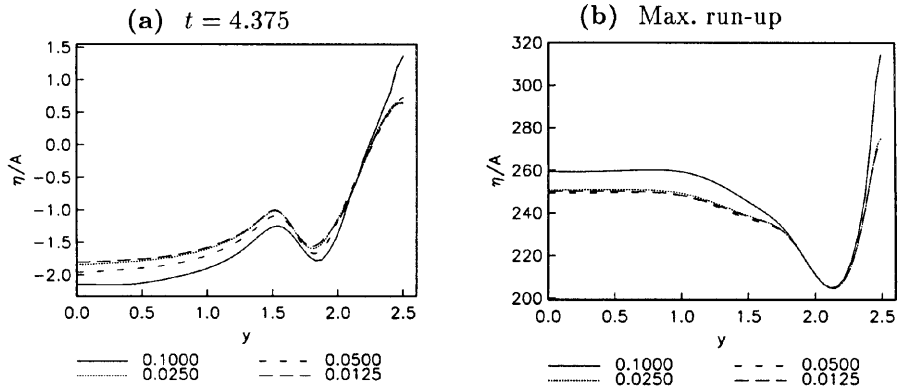

Figure 6. Convergence of elevation of shoreline and maximum amplification for a wave pulse impinging on a point; $\lambda = 2, B = r = 0{\cdot}5, A = 0{\cdot}0175$. Curves are marked by the value of Δx, the average grid size in the cross-shore direction

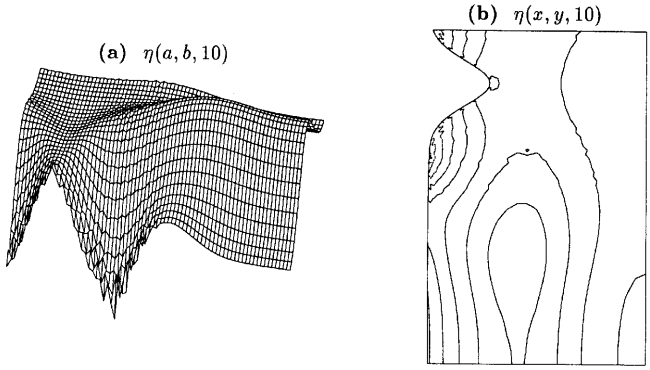

Figure 7. Surface elevation at $t = 10$ for $\lambda = 8, B = 2, r = 1$ and $A = 0{\cdot}02$ as computed by coarse grid $\Delta x = 0{\cdot}28$. (a) Perspective plot for η as function of *Lagrangian* co-ordinates a and b. The field is viewed from a point 'above the shore'. (b) Contour diagram in physical (x, y) co-ordinates, with increment 0·005. To increase readability, we have included part of the region $y > y_p$

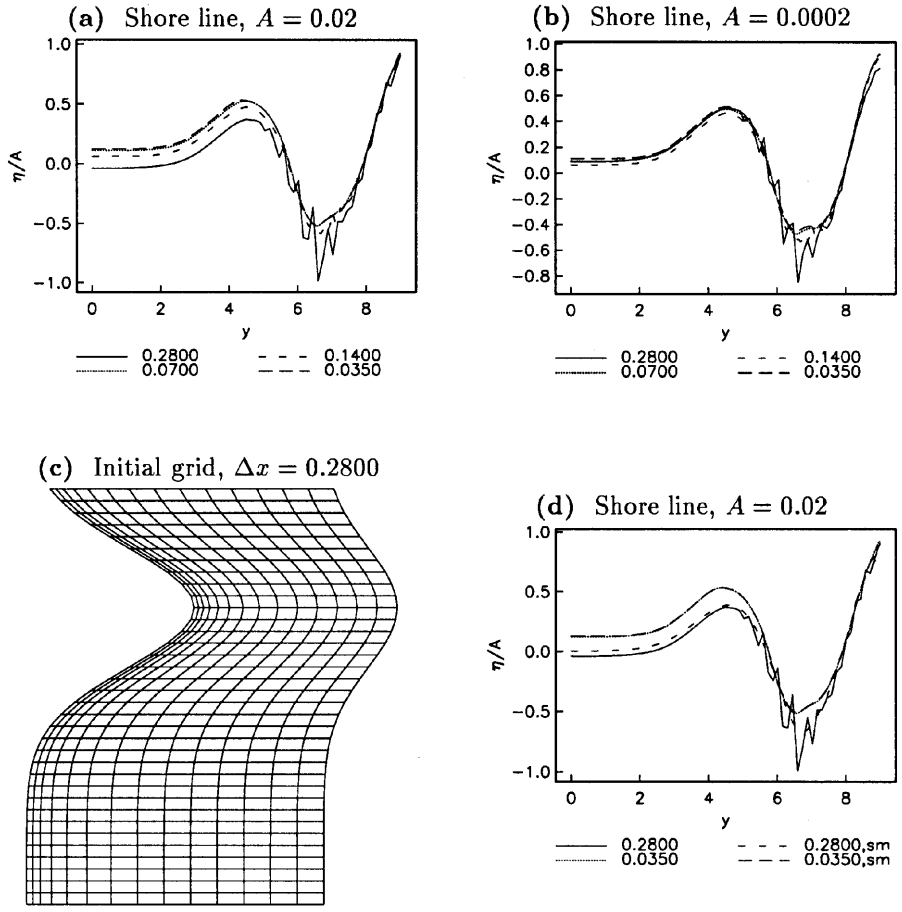

Figure 8. (a, b) Grid refinement tests for a wave pulse impinging on a point; $\lambda = 8, B = 2, r = 1$ at $t = 10$. Curves are marked by the value of Δx. (c) Initial grid distribution around headland for coarsest grid. Again some of the regions $y > y_p$ is depicted. (d) Effect of filtering for two selected grids. Curves for filtered data are marked by 'sm'

6. EXAMPLE 2. WAVE GENERATION BY SLIDES PENETRATING THE FLUID SURFACE

The numerical methods defined by (10)–(13) are easily generalized to include the effect of a time-dependent bottom topography; the explicit dependence on the time t is simply stated in (11). This is utilized in the following example, where we model the wave generation in a fjord or lake due to a landslide penetrating the water.

6.1. Geometry and set-up

The idealized bottom topography selected for this example is an infinitely long fjord or channel. A co-ordinate system with x-axis across the fjord and y-axis at one of the equilibrium shorelines is introduced. The equations are put in non-dimensional form with the width L and maximum depth $h_{\max}$ as horizontal and vertical length scales respectively. The time scale is given by $L/\sqrt{(gh_{\max})}$.

The slide has horizontal extensions $2L_s$ and $2B_s$ across and along the fjord direction respectively and height A. The slide centre starts at (x_0, y_p) and travels a distance R in a time T_R along a line perpendicular to the initial shoreline. The bottom topography is then given by

$$h(x, y, t) = 4x(1 - x) - \hat{h}(x - x_r(t), y - y_p), \tag{24}$$

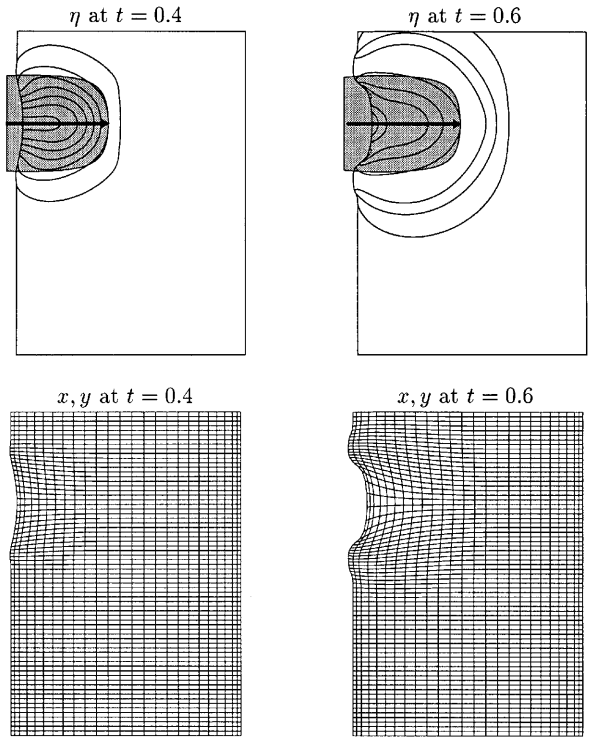

Figure 9. Slide-generated waves in a fjord for $A = 0{\cdot}3$. Upper panels show the surface elevation at $t = 0{\cdot}4$ and $0{\cdot}6$, with contour increment $0{\cdot}03$. Lower panels show the corresponding disturbed grid, with one of four grid points plotted. Shaded regions indicate the location of the slide body, while arrows show the distance covered by the slide. Once more we have also displayed part of the symmetric image above the line $b = y_p$

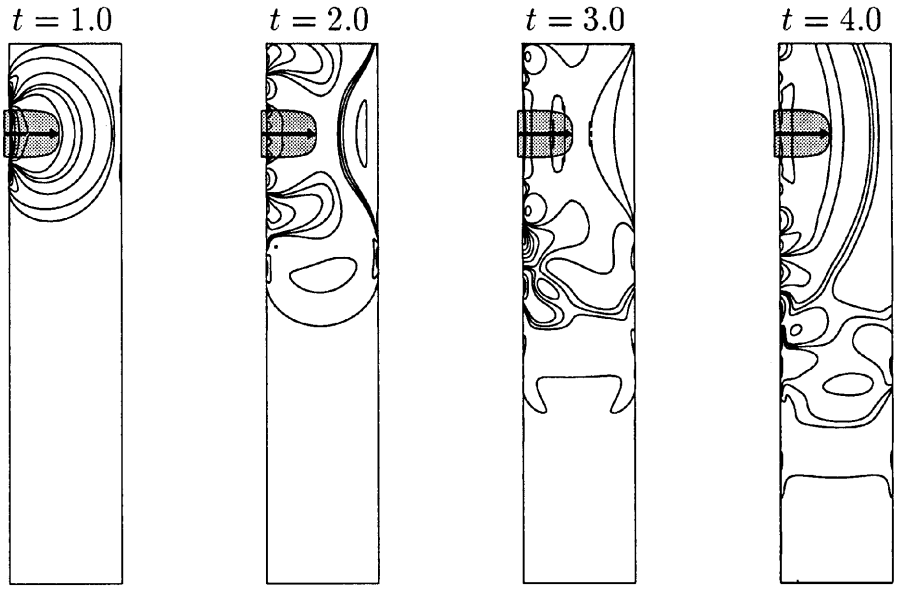

Figure 10. Surface elevation at different times for $A = 0{\cdot}03$. The contour increment is 0·003 and the whole computational domain is depicted together with part of the domain $y > y_p$ as in some preceding figures

where $\hat{h}$ defines the shape of the slide and $x_r(t) = x_0 + 0{\cdot}5R[1 - \cos(t\pi/T_R)]$ is the position of the centre of the slide. For $t > T_R$ the slide remains at rest. The slide body is described by the function

$$\hat{h}(s, p) = A \cos^2\left(\frac{s\pi}{2L_s}\right) \cos^2\left(\frac{p\pi}{2B_s}\right) \tag{25}$$

for $-L_s < s < L_s$ and $-B_s < p < B_s$ and by $\hat{h} = 0$ elsewhere.

6.2. *Simulations*

In the cases presented in this paper, we have chosen $L_s = 0{\cdot}4, B_s = 0{\cdot}24, S = 0{\cdot}5$ and $T_R = 0{\cdot}5$. The slide starts at $x_0 = -0{\cdot}4$; hence the front of the slide is at the shoreline at $t = 0$ and ends up at $x = 0{\cdot}5$, the centre of fjord. In addition to the shores at $a = 0$ and 1, the computational domain is now limited by a symmetry line through $b = y_p$ (centreline of the slide) and $b = 0$. The quantity y_p is chosen large enough to avoid any influence on the solution from reflections at $b = 0$.

Results for the slide height $A = 0{\cdot}3$ are shown in Figure 9. Owing to steepening effects, the head wave breaks before it runs up on the opposite beach and the simulation is stopped.

When A is reduced to 0·03, no breaking occurs until a much longer time. Now we find that waves are reflected back and forth across the fjord (Figure 10), with decreasing amplitude, while a system of waves is propagating along the fjord. This system consists of a fairly symmetric head wave followed by a mixture of wave components with slower transverse celerity.

Some of the latter are edge waves. Although these waves have higher amplitudes than the head wave, their energies are small. A reduction in the horizontal extension of the slide would increase the edge wave generation.

Also for the shoreline motion due to slides we observe good convergence, as shown in Figure 11.

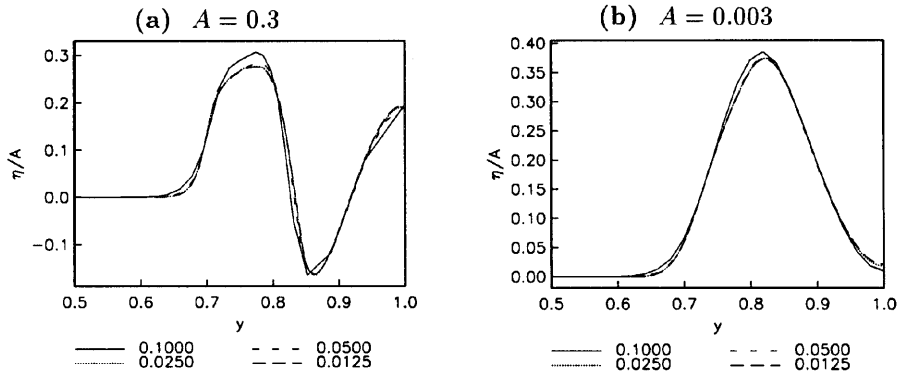

Figure 11. Shoreline elevation for $t = 0{\cdot}6$ and different grids due to a slide. Curves are marked by the value of Δx, the average grid size in the cross-channel direction. (a) Case in Figure 9. (b) Nearly linear case

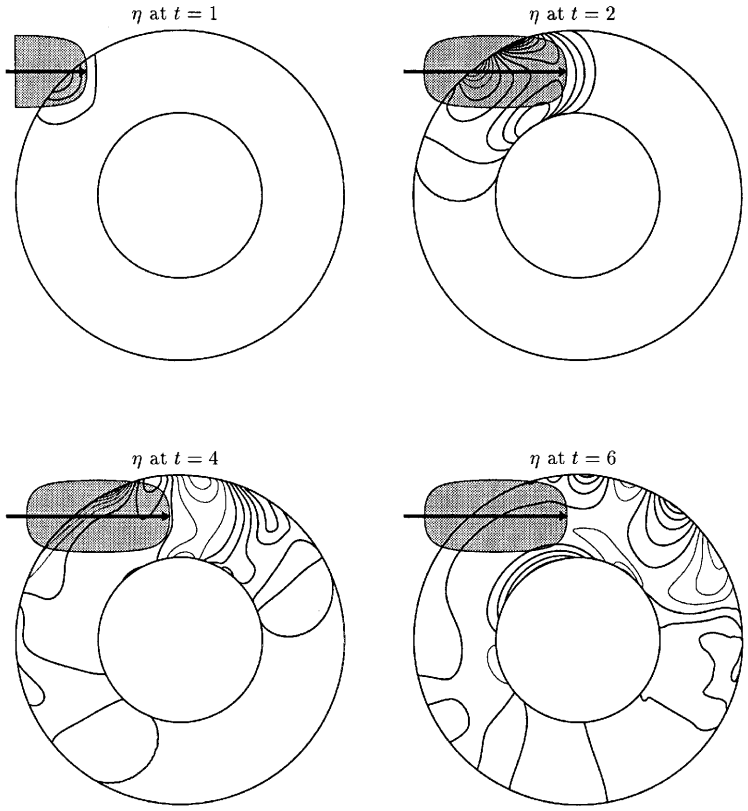

Figure 12. Contour plots of surface elevation (with increment 0·05) for slide in circular lake

7. EXAMPLE 3. RUN-UP IN A CIRCULAR LAKE

The generation of waves due to a landslide penetrating the surface is now studied for a circular lake with a circular island. The island and lake have a common centre; the dimensionless radii are 1 and 2 respectively. The selected bottom topography depends only on the radial co-ordinator r. The profile is parabolic, with zero depth at the shorelines $r = 1$ and 2 and maximum depth unity at $r = 1{\cdot}5$.

A Cartesian co-ordinate system is introduced with its origin at the centre of the island.

The landslide is defined as in the previous example with parameters $L_s = 2, B_s = 1$, $A = 0{\cdot}05, x_0 = -3, y_p = 1{\cdot}5, S = 4$ and $T_R = 2$. Hence the slide centre moves along the chord $y = 1{\cdot}5$ from $x = -3$ to -1. Considering the actual bathymetry, this slide path is not very likely from a physical point of view, but it may still produce interesting physical effects. Figure 12 shows the surface elevation at different times. We note the strong generation of edge waves along the outer shore, which is partly due to the slide direction.

8. CONCLUSIONS

The performance of the Lagrangian technique for run-up calculations has been tested on a few selected problems. Each problem is intended to demonstrate some particular features of the method and is subjected to grid refinement tests.

In the first test problem, numerical solutions for two-dimensional standing waves on an inclined plane are compared with the classical solution of Carrier and Greenspan.[1] Besides verification of the code, the main objective of the comparison is to unravel the effect of the shore-line singularity on the convergence in the nearly linear as well as the strongly non-linear case. In deep water the numerical technique is of second order, which is easily established by Taylor series expansion. However, the application of corresponding arguments at the shore is not straightforward. For small amplitudes we still find a convergence rate at the shoreline that is nearly quadratic. When the amplitude is increased, the convergence becomes slower, as expected. Nevertheless, even for waves that are close to breaking at the shore, we observe good and robust convergence of the method.

In the second problem, concerning a finite length pulse impinging on a headland, we study the effects of curved coastlines and near-shore diffraction. In spite of its simplicity, this problem involves a number of interesting physical features that are discussed briefly. Our simulations demonstrate the importance of selective grid refinement in the coastal zone and that this zone is particularly exposed to effects akin to aliasing. However, the noise production is basically a linear diffraction effect that can be linked to the fact that even small misrepresentations of the depth may lead to large relative variations in the optical density in the vicinity of the shore. Hence similar behaviour must be expected also for other finite difference formulations. The evolution of the resulting short-scale noise is effectively removed through grid refinement or suppressed by a gentle filtering that corresponds to horizontal diffusion. Again the method displays robust convergence, even for rather 'pointed' headlands that lead to skew grids. Probably the accuracy of the method would have been improved by searching an optimal grid. However, such a grid may be difficult to construct in even slightly more complex geometries.

A slide penetrating the fluid surface is a problem of principal physical importance. It is easily implemented within the Lagrangian technique but will introduce the new problem of a strongly non-linear forcing at the shoreline singularity. Still, our simulations display no specific problems related to the slide/fluid tip interaction. On the contrary, the numerical technique handles a high degree of dynamic grid distortion at the shore with good accuracy.

The last example again concerns wave generation by a slide, but this time in a more complex lake geometry. This case represents one of the geometries effectively handled by a simple grid. Very

complex geometries probably require either the introduction of a nesting technique or the application of finite elements. In some cases also dynamic regridding must be considered. The authors plan to pursue some of these aspects in future work.

For the presented examples the results of the run-up model have been very promising and indicates that the method, already at this stage, is well suited for obtaining accurate solutions for problems of medium complexity.

REFERENCES

1. G. F. Carrier and H. P. Greenspan, 'Water waves of finite amplitude on a sloping beach', *J. Fluid Mech.*, **4**, 97–109 (1958).
2. G. F. Carrier, 'Gravity waves on water of variable depth', *J. Fluid Mech.*, **24**, 641–659 (1966).
3. B. Gjevik and G. Pedersen, 'Run-up of long waves on an inclined plane', *Preprint Ser. Dept of Maths, University of Oslo, 2/81*, 1981.
4. C. E. Synolakis, 'The run-up of solitary waves', *J. Fluid Mech.*, **185**, 523–545 (1987).
5. C. E. Synolakis, M. K. Deb and J. E. Skjelbreia, 'The anomalous behaviour of the run-up of cnoidal waves', *Phys. Fluids*, **31**, 3–5 (1988).
6. R. E. Meyer and A. D. Taylor, 'Run-up on beaches', in *Waves on Beaches and Resulting Sediment Transport*, Ed. R. E. Meyer, Academic, 1972, pp. 357–411.
7. W. C. Thacker, 'Some exact solutions to the nonlinear shallow-water wave equations', *J. Fluid Mech.*, **107**, 499–508 (1981).
8. S. Hibberd and D. H. Peregrine, 'Surf and run-up on a beach: a uniform bore', *J. Fluid Mech.*, **95**, 323–345 (1979).
9. Z. Kowalik and T. S. Murty, 'Numerical simulation of two-dimensional tsunami runup', *Marine Geodesy*, **16**, 87–100 (1993).
10. R. A. Flather and N. S. Heaps, 'Tidal computations for Morecambe bay', *Geophys. J. R. Astron. Soc.*, **42**, 489–517 (1975).
11. G. Pedersen, 'Grid effects on tsunamis in nearshore regions', *Preprint Ser. Dept of Maths, University of Oslo, 1/95*, 1995.
12. B. Gjevik and G. Pedersen, 'Numerical simulation of run-up of long water waves', *Proc. Int. Symp. on Refined Modelling of Flows*, Paris, 1982, 9pp.
13. G. Pedersen and B. Gjevik, 'Run-up of solitary waves', *J. Fluid Mech.*, **135**, 283–299 (1983).
14. G. Pedersen, 'Run-up of cnoidal waves', *Preprint Ser. Dept of Maths, University of Oslo, 4/87*, 1987.
15. J. A. Zelt and F. Raichlen, 'A Langrangian model for wave-induced harbour oscillations', *J. Fluid Mech.*, **213**, 203–225 (1990).
16. S. Grilli and I. A. Svendsen, 'Runup and reflection of a solitary wave on steep slopes in a numerical wave tank', *Proc. Fourth Int. Workshop on Water Waves and Floating Bodies*, Ed. J. Grue, Dept of Mathematics, University of Oslo, Oeystese, 1989, pp. 77–80.
17. S. Grilli and I. A. Svendsen, 'Computation of nonlinear wave kinematics during propagation and run-up on a slope', *NATO ASI Ser. E*, **178**, 378–412 (1990).
18. F. Mesinger and A. Arakawa, *Numerical Methods Used in Atmospheric Models*, WMO Vol. 17, GARP, 1976, 64pp.
19. E. Pelinovksy, O. Kozyrev and E. Troshina, 'Tsunami runup in a sloping channel', *Proc. Int. Workshop on Long Wave Modelling*, Seattle, WA, 1995.
20. J. W. Miles, 'Resonantly interacting solitary waves', *J. Fluid Mech.*, **79**, 171–179 (1977).
21. R. L. Wiegel, 'Water wave equivalent of Mach-reflection', *Proc. 9th Conf. on Coastal Engineering*, Vol. 6, ASCE, 1964, pp. 82–102.

